Chapter

Fractal and Polar Microstrip Antennas and Arrays for Wireless Communications

Paulo Fernandes da Silva Junior, Mauro Sérgio Pinto Silva Filho, Ewaldo Eder de Carvalho Santana, Paulo Henrique da Fonseca Silva, Elder Eldervitch Carneiro de Oliveira, Maciel Alves de Oliveira, Fabrício Ferreira Batista, Alexandre Jean René Serres, Raimundo Carlos Silvério Freire, Almir Souza, Silva Neto, Severino Aires de Araújo Neto and Carlos Augusto de Moraes Cruz

Abstract

This chapter presents the research done by authors in recent years on microstrip antennas and their applications in wireless sensors network. The subject is delimited to the study of conventional microstrip antennas, from which antennas with fractal and polar shapes are proposed. A detailed description of the antenna design methodology is presented for some prototypes of microstrip antennas manufactured with different dielectric substrates. Analysis of the proposed antennas has been done through computational simulation of full-wave methods. Experimental characterization of antennas and dielectric materials has been performed with the use of a vector network analyzer. The results obtained for the resonant and radiation parameters of the antennas are presented. Computer-aided design (CAD) of microstrip antennas and arrays using fractal and polar geometrical transformations results in a wide class of antenna elements with desirable and unique characteristics, such as compact, exclusive, and esthetic antenna design for multiband or broadband frequency operation with stable radiation pattern.

Keywords: fractal-shaped antennas array, polar-shaped antennas, wearable antennas, dielectric resonator antennas, wireless sensor network

1. Introduction

From the 1990s, with the advent of the Internet, the popularization of portable terminals (laptops, mobile phones, etc.) favored the telecommunications industry, and the infrastructure of networks experienced a remarkable growth [1, 2]. When the information age emerges from an increasingly networked world, the digital

information and communication technology permeate the society and are increasingly important to their development [3, 4]. Modern wireless applications demand esthetic, multifunctional, portable terminals (laptops and smartphones) that operate in multiple frequency bands and can integrate different wireless services: 4G, Wi-Fi, Bluetooth, NFC, GPS, etc. Future trends toward 5G systems also require enhanced mobile broadband for emergent applications, as wireless sensors network [5].

With the rapid advance of wireless communication systems, the use of antennas in base stations and portable terminals must meet increasingly stringent criteria, such as miniaturization, integration with other systems, and multiband or broadband operation [1–4]. Due to its attractive features, low-profile microstrip antennas (MSA) and arrays are well suitable to meet the demands of fixed or mobile wireless applications [6–10].

Antenna parameter specifications change according to application. Indeed, fixed antennas must have high gain, stable radiation pattern, and bandwidth tolerance; embedded antennas should be efficient in radiation and possess larger beam width [3]. In short-range UWB wireless systems, the antenna bandwidth exceeds the lesser of 500 MHz or 20% of the center frequency [11, 12]. Thus, impedance bandwidth, gain, radiation pattern, and polarization are fundamental parameters for antenna designers to take into account.

A trend in the application of antennas for modern wireless systems is the use of compact antennas with stable radiation coverage over a wideband [2–4]. An antenna must be compact in many situations: embedded antennas, wearable antennas, camouflaged antennas, etc. However, most often an antenna electrically small narrows the impedance bandwidth, reduces gain, and limits control of the resulting radiation pattern [6, 10].

This chapter discusses the design of innovative microstrip antennas with fractal and polar shapes, which has been optimized for wireless sensors network applications. To show the advantages and disadvantages of proposed antennas, their resonant and radiation properties are compared with that presented by conventional MSAs. The antenna types addressed include patches and printed monopoles. Further developments include microstrip feeding techniques, dielectric resonator antenna (DRA), esthetic wearable antennas, and antenna arrays.

2. Microstrip antennas: types, applications, and design methodology

2.1 Types and applications

Since the concept of microstrip radiators was introduced by Deschamps in 1953, microstrip antennas only were manufactured in the 1970s with the use of the printed circuit technology (PCB) by Byron, Munson, and Howell [13–16]. Since then, microstrip antennas have been a subject of extensive research and development for military and commercial applications.

The most common type of microstrip antenna is the so-called patch antenna, which is fabricated with PCB technology by etching the shape of radiating patch above a dielectric substrate backed by a ground plane. Conventional patch shapes that result in narrowband and wide-beam antenna include square, rectangular, circular, and elliptical. Patch antennas have a low profile and can be mechanically robust and shaped to conform to the curving surfaces or embedded into portable terminals.

From the initial concept introduced in [13], a variety of MSA has been proposed to meet the operating requirements in modern wireless applications. **Figure 1** illustrates some examples of these antennas fabricated using PCB technology for different types of excitation: microstrip, CPW, coupled, and coaxial.

The operating bandwidth of an antenna is an initial design specification of paramount importance to the antenna designer. The frequency bands defined for some

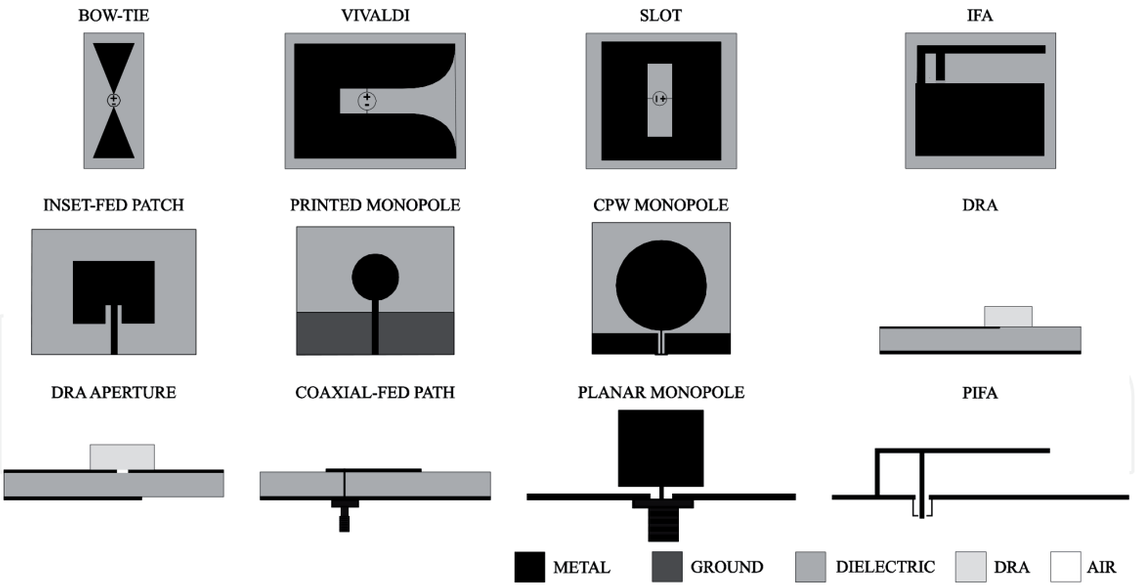

Figure 1.
Antennas manufactured using the PCB technology.

Application	*Center Frequency*	*BW (MHz)*	*BW (%)*
NFC	13.560 MHz	13.553-13.567	0.1
GPS	1575.42 MHz	1563-1587	1.5
3G (UMTS)	1900 MHz	uplink (1920-1975)	2.8
	2100 MHz	downlink (2110-2165)	2.6
4G (LTE)	700 MHz (708-803 MHz)	uplink (708-748)	5.5
		downlink (763-803)	5.0
	2.5 GHz (2500-2690 MHz)	uplink (2500-2570)	2.7
		downlink (2570-2620)	1.9
		downlink (2620-2690)	2.6
Wi-Fi (IEEE80211b,g)	2.45 GHz	2400.0–2483.5	3.4
Wi-Fi (IEEE80211a)	5.8 GHz	5150-5350 (*indoor*)	3.8
		5470-5725	4.5
		5725-5850	2.2
UHF TV	638 MHz	470-806	52.6
UWB	6.85 GHz	3100-10600	109.5

Table 1.
Frequency bands of wireless communication services.

wireless applications are shown in **Table 1**. Conventional patch antennas suffer with narrow impedance bandwidth, low gain, and low power handling capability [6]. However, patch antennas have been applied for portable devices and base stations. A challenge for the designer is to enhance the patch antenna impedance bandwidth without compromising its radiation properties. A variety of broadband techniques for patch antennas can be found in the literature [3, 4, 9].

The microstrip antennas (IFA, Inverted-F Antenna, and PIFA, Planar Inverted-F Antenna) are widely used in wireless communication terminals [2–4]. Printed monopole antennas are very popular in ultra-wideband applications [3]. Discrete patch or monopole radiators can be arranged in versatile arrays to improve bandwidth and directivity or to synthesize a given radiation pattern [6–10].

Fractal antennas have a natural multiband behavior and compact design and can be used as a reconfigurable microstrip antenna [17–19]. Optimized fractal antennas in size and performance are suitable for wireless applications [20]. Currently, fractal antennas have several commercial applications, and international companies such as Fractal Antenna Systems, Fractus, Rayspan, and Ficosa International, among others, explore the unique properties of fractals for the manufacture of commercial antennas. Recently, polar shape commercial antennas inspired by the Gielis formula have also been proposed [21].

2.2 Microstrip antenna design methodology

In this section, a microstrip antenna design methodology using PCB technology is presented, and preliminary results are presented. After choosing a type of MSA, its design had been done in order to meet the application criteria. Often, design requirements are conflicting, for example, when a small-volume antenna with a wide bandwidth and high gain is desired.

The design of conventional patch antennas (with square, rectangular, circular shapes) is already well established [6]. In general, the initial patch dimensions are given by analytical expressions obtained from approximated models, for example, the cavity model [6].

After initial design phase, an accurate analysis of the resonant and radiation antenna properties is made through computer simulation of a full-wave method: MoM, FDTD, FEM, etc. At this step, the initial dimensions of an antenna (radiator, feed line, ground plane, etc.) can be adjusted by designer for fine tuning of resonant frequency, bandwidth, and gain, among other parameters.

A trend in the development of microstrip devices involves an intensive use of computational resources available in the application of CAD tools, computational electromagnetic analysis methods, as well as computational intelligence tools for modeling and optimization [22, 23]. **Figure 2** shows a block diagram with the main steps of the methodology used in the development of microstrip antenna prototypes.

In this design approach considered, the microstrip antennas built on single dielectric layer are fed by microstrip lines. Computational simulations of microstrip antennas were done with the use of commercial software ANSYS Designer®. A developed FDTD-3D method also is applied for antenna analysis.

MSA manufacture was performed using two PCB techniques: corrosion with iron perchloride and with a milling machine, model LPKF ProtoMat S103. **Figure 3(a)**

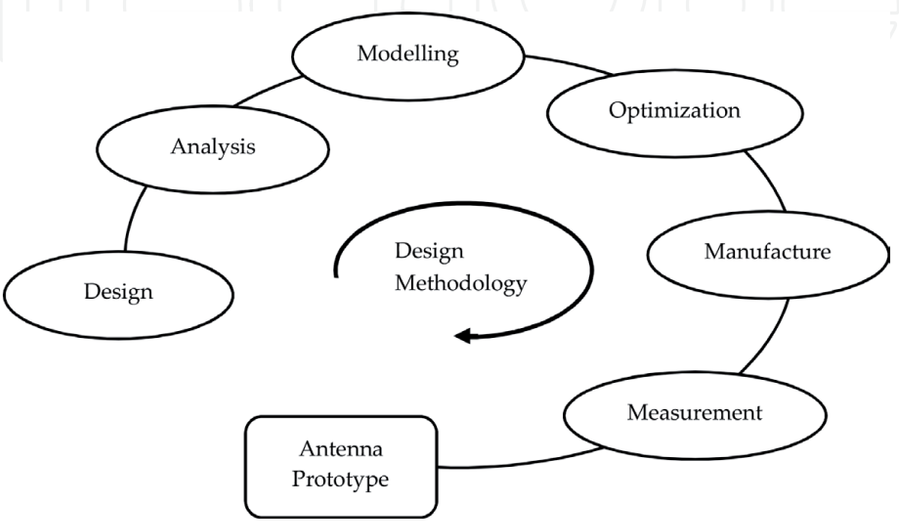

Figure 2.
Design methodology for microstrip antennas.

shows enlarged images of microstrip bends and T-junctions made using chemical corrosion and milling machine, whose manufacturing results are more accurate. Measured values of antenna parameters were obtained using a vector network analyzer (model S5071C, Agilent Technologies).

Relative dielectric permittivity and loss tangent of dielectric materials can be obtained by the following methods: coaxial probe, free space, resonant cavities, and capacitive methods [24]. The characterization of the dielectric materials (ceramic, polyamide, and denim) was performed by probe method using E5071C VNA (300 kHz–20 GHz) and Dielectric Probe 85,070 program, **Figure 3(b)**. **Figure 4(a)** shows results for ceramic dielectric. **Figure 4(b)** shows results of a compact and broadband inset-feed DRA antenna for operation in 2.4 GHz band. A list of dielectric material parameters addressed in this work is presented in **Table 2**.

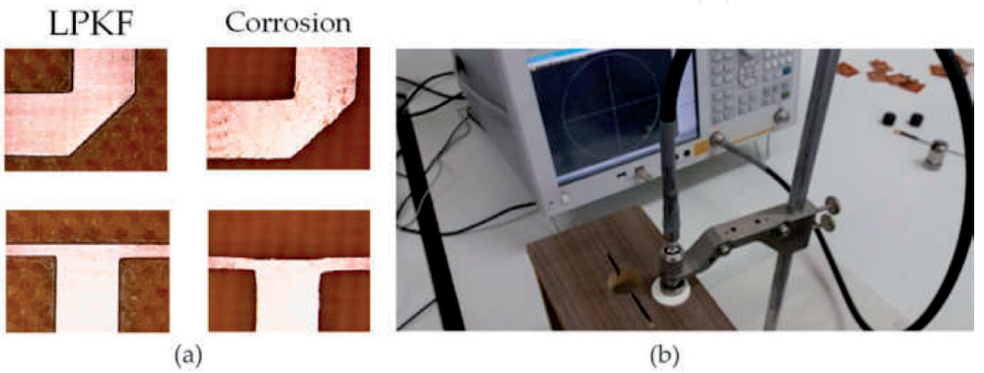

Figure 3.
(a) Images of PCB results; (b) ceramic characterization with dielectric probe 85,070.

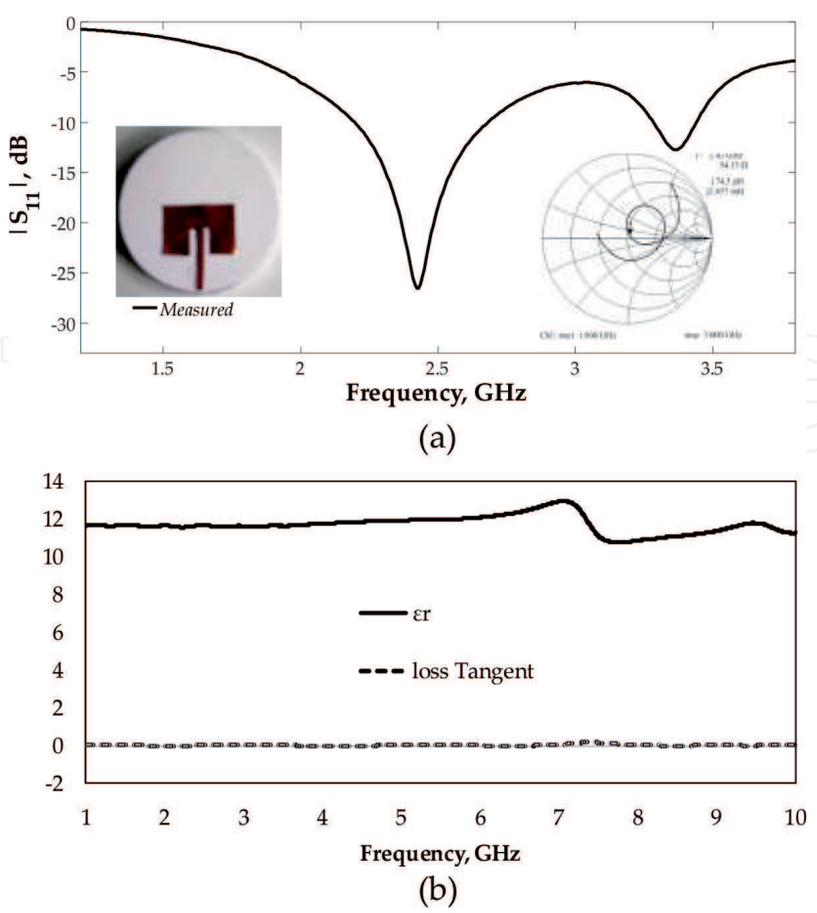

Figure 4.
DRA: (a) measured ceramic material parameter; (b) compact and broadband 2.45 GHz.

Dielectric Material	*Cost*	ε_r	*tan (δ)*	*h (mm)*
Fiberglass	low	4.40	0.002	1.55
Glass epoxy	low	5.2	0.002	1.55
Duroid	medium	2.2	0.0004	1.57
Ceramic (Calcium Titanate – $CaTiO_3$)	high	12	0.006	8
Polyamide	low	4	0.004	0.005
Denim	low	2.12	0.08	1

Table 2.
List of dielectric materials.

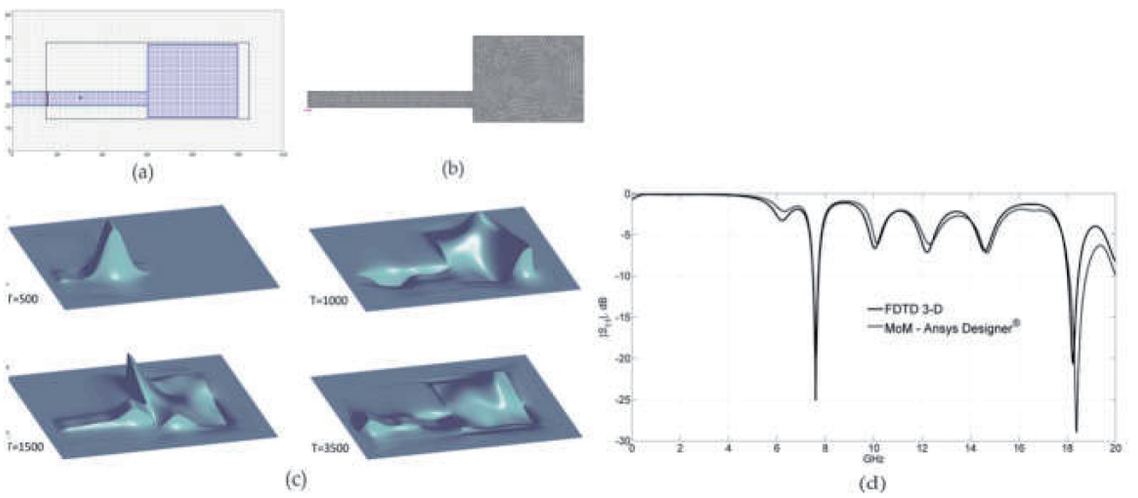

Figure 5.
Microstrip patch antenna analysis: (a) FDTD, uniform mesh; (b) MoM, tetrahedral mesh; (c) Ez-field propagation in the time domain; (d) comparison between simulation results.

Figure 5 shows analysis results for a benchmark patch antenna proposed by Sheen [25]: using a homemade FDTD-3D method, developed according to [26], and using Ansys Designer (MoM). Sheen's antenna geometry is illustrated in **Figure 5(a)** superimposed by the rectangular uniform FDTD mesh; MoM tetrahedral mesh is shown in **Figure 5(b)**.

The FDTD simulation makes it possible to observe the electromagnetic fields in the time domain. The Ez-field propagation in dielectric layer of an incident Gaussian pulse is illustrated in **Figure 5(c)**. After the occurrence of multiple reflections in the patch contours, the reflected wave back through the microstrip line is used to compute the reflection coefficient. In **Figure 5(d)** the obtained analysis results in the frequency domain are compared. The simulation time of each method depends on the computational mesh, and in this example run, it is about 15–30 minutes, which is a computing time lower than that spent in 1990 by Sheen, 12 hours [25].

Figure 6 illustrates the square patch antennas designed to operate at 2.45 GHz considering different types of microstrip line feeding techniques (direct, quarter-wave transformer, inset-fed). A combination of these feeding techniques also proposed for impedance matching of patch antenna, **Figure 6(d)**. In addition, spurline filter can be inserted into the microstrip line feed for harmonic rejection with minimum degradation of the antenna radiation pattern, **Figure 6(e)**.

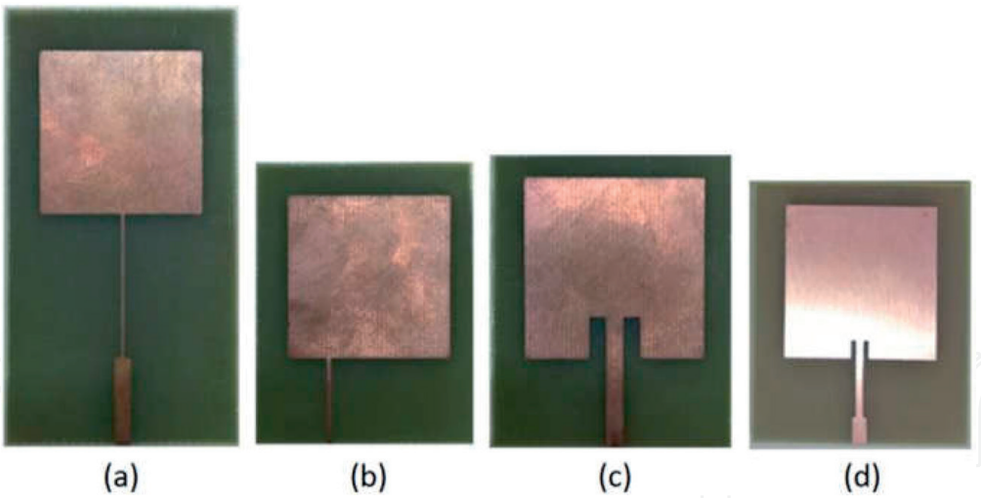

Figure 6.
Square patch antennas and microstrip line feed techniques: (a) direct, (b) QWT, (c) inset-feed, (d) hybrid, (e) hybrid with double-arm spurline filter.

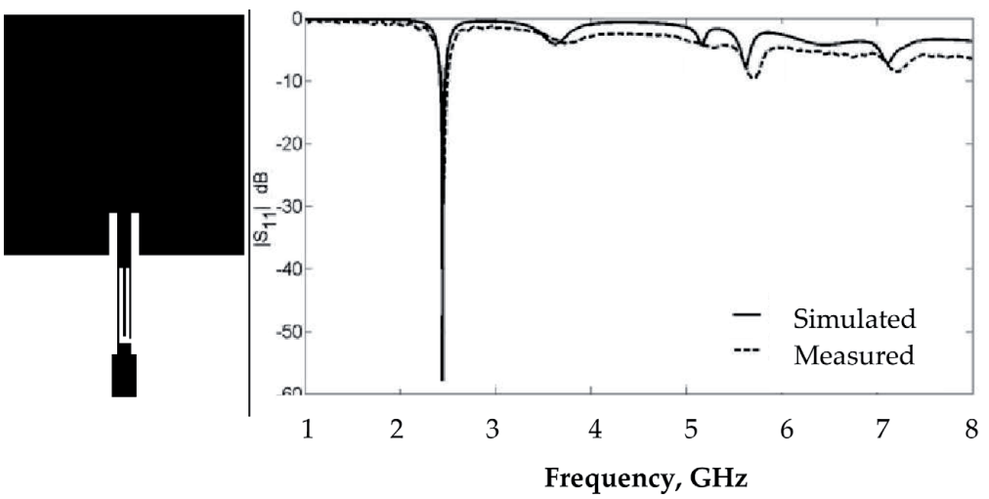

Figure 7.
(a) Layout of 2.45 GHz single-band square patch antenna, (b) simulated and measured results for reflection coefficient.

The inset-feed and QWT techniques have been combined to obtain a hybrid impedance matching with wider microstrip line section. We insert the spurline band-stop filter in QWT microstrip line section in order to suppress high-order patch resonances. **Figure 7(a)** shows layout and dimensions of such antenna considering low-cost FR-4 fiberglass dielectric substrate (see **Table 2**). **Figure 7(b)** shows simulated and measured results for proposed single-band 2.45 GHz square patch antenna.

3. Fractal and polar transformations

3.1 Types and applications

From a mathematical point of view, a fractal refers to a set in Euclidean space with specific properties, such as self-similarity or self-affinity, simple and recursive definition, fractal dimension, irregular shape, and natural appearance [27]. Fractal geometry is the study of sets with these properties, which are too irregular to be described by calculus or traditional Euclidian geometry language [27, 28].

Fractals are resorted to conventional classes, such as geometrical fractals, algebraic fractals, and stochastic fractals [29]. Two common methods used to generate mathematical fractals are iterated function systems (IFS) and Lindenmayer systems [27–30].

IFS method used to generate a 2-D fractal consisting of a collection of affine transformations with probability given by (1). Affine transformations are most commonly used in IFS. The coefficients of a two-dimensional affine transformation represent the IFS code for scaling, rotations, and translations. An affine transformation of a point to the point is given in (2).

$$\begin{cases} T_1: & (a_1,\ b_1,\ c_1,\ d_1,\ e_1,\ f_1,\ P_1) \\ T_2: & (a_2,\ b_2,\ c_2,\ d_2,\ e_2,\ f_2,\ P_2) \\ \vdots & \vdots \\ T_m: & (a_m,\ b_m,\ c_m,\ d_m,\ e_m,\ f_m,\ P_m) \end{cases} \tag{1}$$

$$\begin{cases} x_{n+1} = ax_n + by_n + e \\ y_{n+1} = cx_n + dy_n + f \end{cases} \tag{2}$$

IFS algorithm consists of four steps: (i) start with an arbitrary point in the plane p0 = (x0, y0); (ii) pick a random transformation, Tm, according to the probabilities, Pm; (iii) transform the point p1 = Tm (p0) and plot it; and (iv) go to step 2. IFS algorithm is continued ad infinitum (for ideal fractal) or until a given number of fractal iterations is reached (for pre-fractals).

Lindenmayer system (or L-system) was initially conceived to model growth phenomena in biological organisms [31]. An L-system grammar handles an initial string of symbols (axiom) and includes a set of production rules that may be applied to the symbols (letters of the L-system alphabet) to generate new strings. A graphic interpretation of strings, based on turtle geometry, is described in [29, 32]. A state of the turtle is defined as a triplet (xk, yk, φk) where coordinates (xk, yk, φk) and angle φk represent the turtle's position and direction, respectively, (3).

$$\begin{cases} x_{k+1} = x_k + d\cos(\varphi_k) \\ y_{k+1} = x_k + d\sin(\varphi_k) \end{cases} \tag{3}$$

The simplest class of L-systems is termed deterministic and context-free or DOL-systems [29, 32]. DOL-system is defined as a triple $H = (V, \omega, \Pi)$, where V is the L-system alphabet, ω is the axiom word, and Π is a finite set of productions. Formal definitions of D0L-systems and their operation can be found in [29, 32]. Given the initial state of turtle (x_0, y_0, φ_0), step size d, and the angle increment $\Delta\varphi$, the turtle can respond to the commands in L-system strings $v \in V$ and represented by the following symbols [29, 32]:

F → Move forward a step of length d, and change state of the turtle according to (3). A line segment between points (x_k, y_k) and (x_{k+1}, y_{k+1}) is drawn.

f → Move forward a step d without drawing a line. The turtle state changes as above.

+ → Turn right by angle $\Delta\varphi$. The next state of the turtle is given by $(x_k, y_k, \Delta_k + \varphi_k)$.

- → Turn left by angle $\Delta\varphi$. The next state of the turtle is given by $(x_k, y_k, \varphi_k - \Delta_k)$.

In **Figure 8**, four examples of fractal iterations using IFS and L-system are shown.

Like fractals, polar transformations give rise to a wide class of shapes. A polar transformation is defined in this chapter through a vector function $\vec{v}(t) = (x(t), y(t)),\ t \geq 0$,

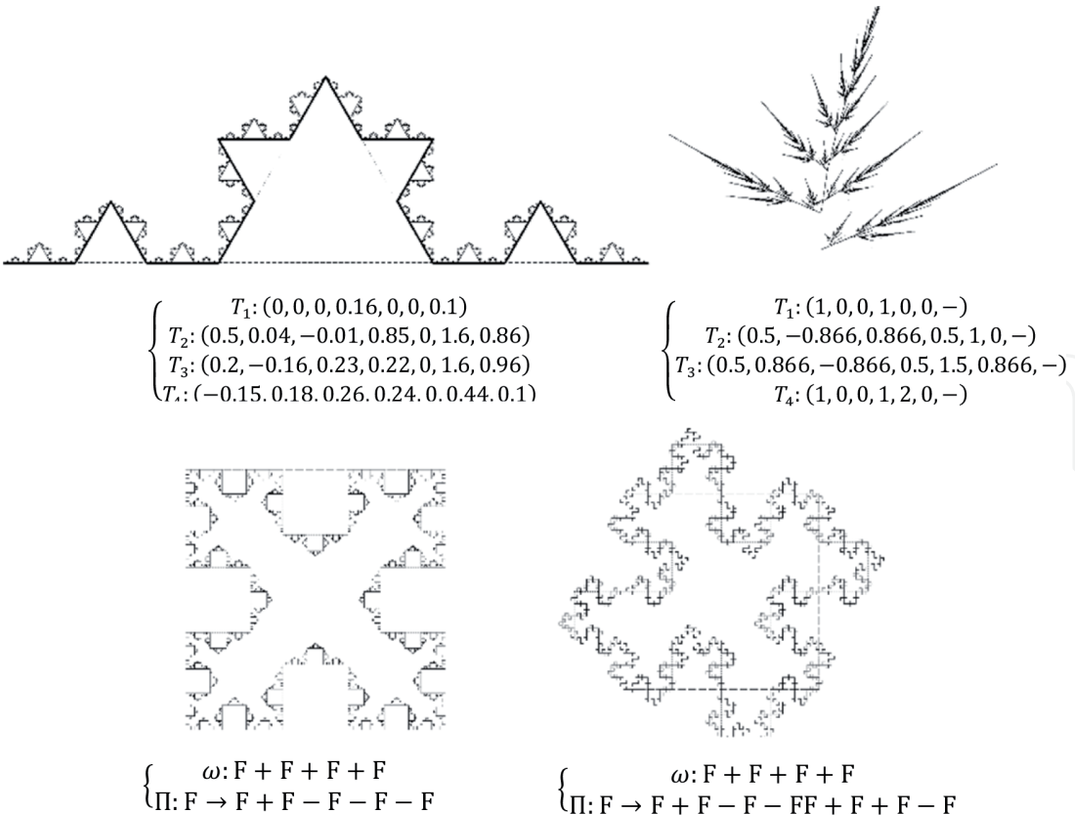

Figure 8.
IFS and L-system pre-fractals: (a) Koch curve; (b) modified Barnsley fern; (c) Koch Island; (d) Minkowski Island.

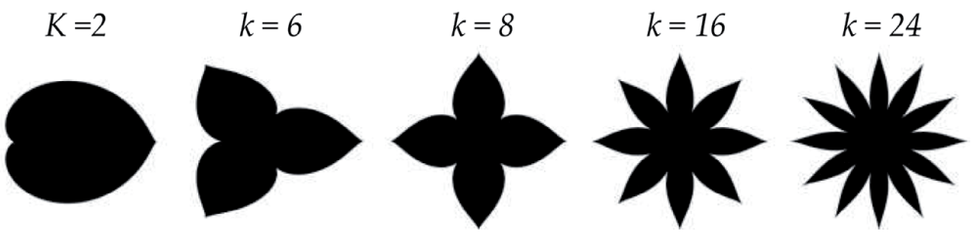

Figure 9.
Esthetic polar transformation for k varying up to k = 32 petals in (5).

that is, for each real value, t is associated with a vector in $\Re^2$, (4). An example of an esthetic polar transformation defined by (5) is presented in **Figure 9** for k varying up to k = 32 petals.

$$\begin{aligned} &\vec{v}(t): I \to \Re^n \\ &t \to \vec{v}(t) \end{aligned} \tag{4}$$

$$\vec{v}(t) = \left(1 + \frac{\cos(t)}{2}\right) \cdot \left(\cos\left(\frac{2t - sen(2t)}{k}\right), \sin\left(\frac{2t - sen(2t)}{k}\right)\right), \quad 0 \le t \le k\pi \tag{5}$$

4. Fractal and polar-shaped microstrip antenna

4.1 Koch fractal microstrip antenna

The design of pre-fractals patch antennas has been a subject of great interest to designers and researchers in the field of antennas. Previously published

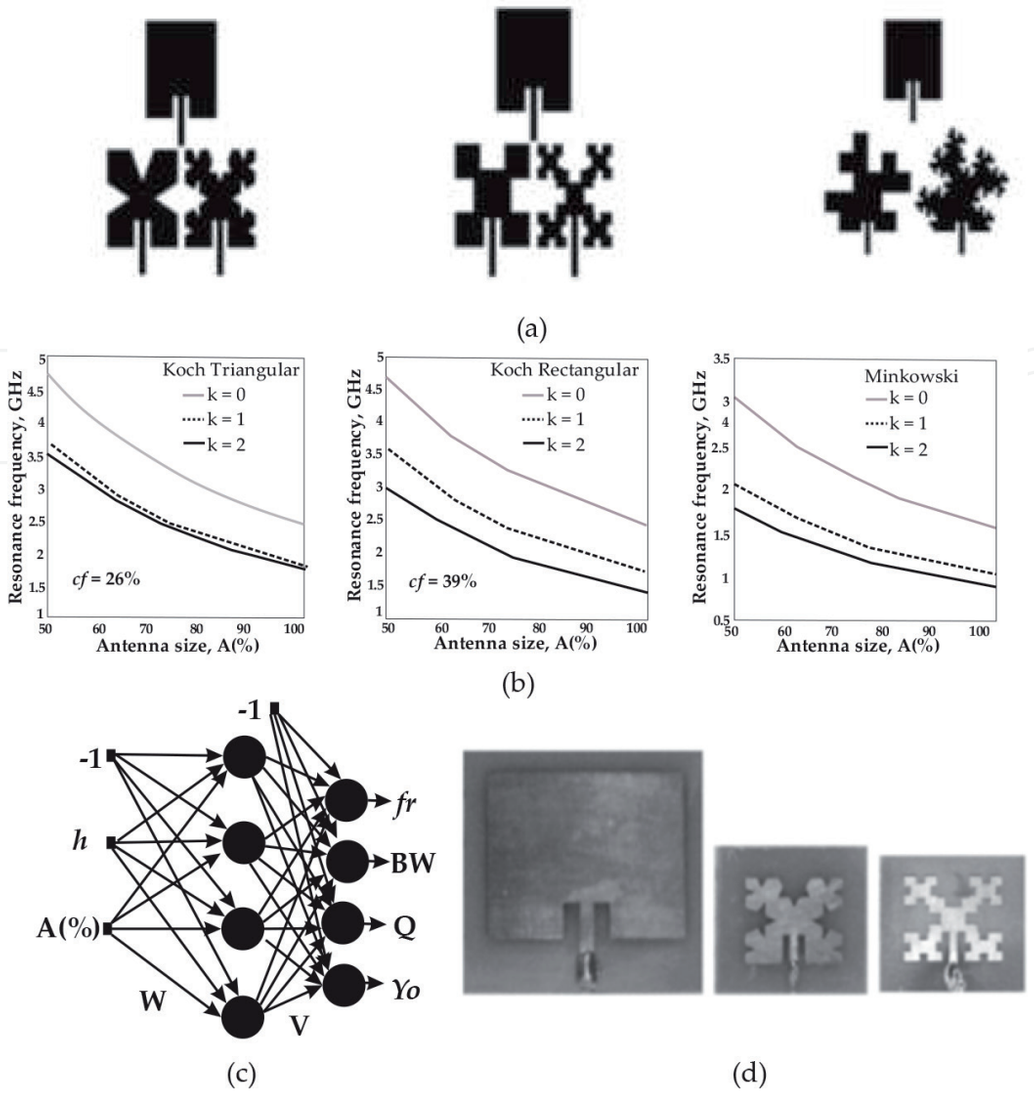

Figure 10.
Pre-fractals patch antennas: (a) image layouts; (b) parametric analysis; (c) neuromodeling; (d) image comparing overall sizes of the built patch antennas—Rectangular and pre-fractals.

works by the authors have contributed to this research area, showing the miniaturization of inset-fed patch antennas with the use of Koch and Minkowski pre-fractals [13, 19, 33], **Figure 10(a)**. Frequency compression factors of 26.1, 39, and 42% were observed for level 2 pre-fractals: triangular Koch, rectangular Koch, and Minkowski, respectively [13, 19, 33]. Pre-fractal patch antennas are defined with two fractal parameters: iteration number (level) and scaling factor. They possess a large design region of interest, **Figure 10(b)**; are easy to model using neural network, **Figure 10(c)**, [19]; and their shapes and multiband behavior facilitate frequency reconfiguration [5]. The unique properties of geometric fractals are useful to synthesis of more compact patch antennas, **Figure 10(d)**, [13, 19, 33, 34].

4.2 Wearable teragon antennas

The use of wearable antennas is necessary that have some characteristics as: easy interaction with the body, low visual impact, preferably low cost, and flexible structure [19]; for this reason, the materials used in the manufacture of the wearable antennas must follow some requirements: easy interaction with the body, flexible structure, reduced visual impact, and preferably low cost [19].

Teragon was a term coined by Mandelbrot that literally means, "monster curve" [28]. The proposed wearable teragon patch antennas are based on a square patch antenna with displaced microstrip line feed. Square patch antenna dimensions are calculated according to [13, 28, 34]. Pre-fractal teragons were developed with a scale factor of R = 6 and number of copies, n = 18. **Figure 11(a)** shows dimensions and shapes of the teragons. Images of built antenna prototypes with polyamide flexible dielectric substrate are shown in **Figure 11(b)**. Obtained simulated and measured results for reflection coefficient and gain are shown in **Figure 12**.

Figure 12a shows the comparison between simulated and measured reflection coefficient of the wearable flexible antennas. The increase of the patch perimeter by the use of teragon shapes provides a reduction of the resonant frequencies. The main highlight is for teragon 1, with reduction of approximately 1 GHz, when compared to the initial square patch antenna.

The gain (dB) simulated in resonant frequencies of the wearable path antennas is shown in **Figure 12b**. As noted, the gain is reduced when fractal level increase. The initial square patch antenna presented higher gain, with maximum gain in end-fire direction of 6.13 dBi, and the teragon 1 showed the maximum gain of 4.26 dBi (**Figure 12b**).

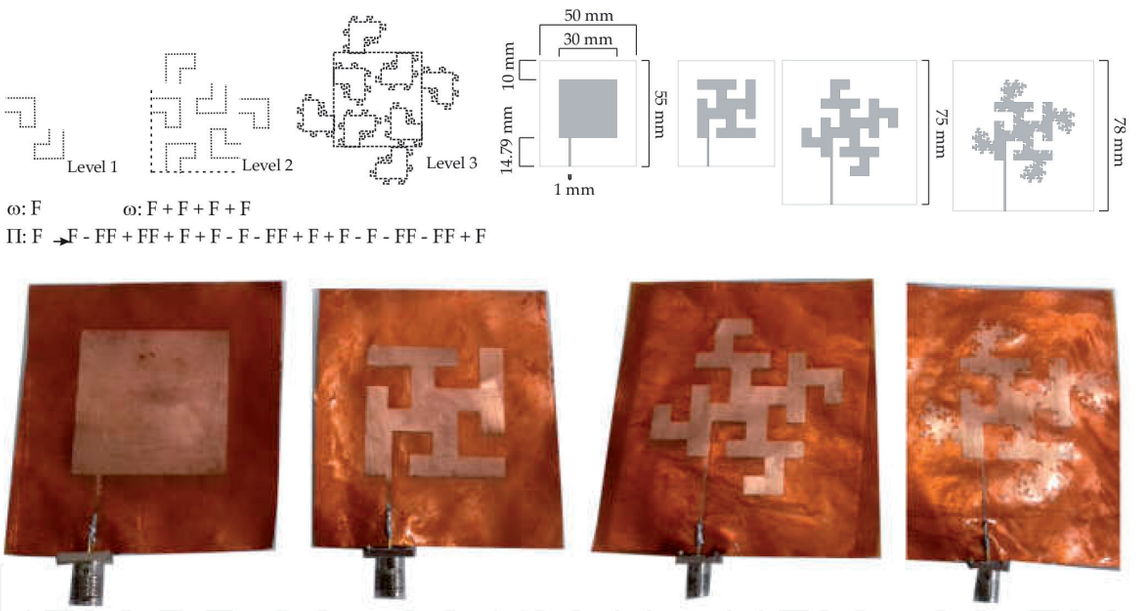

Figure 11.
Pre-fractal teragon patch antenna design steps (a) Matlab dxf images, (b) layouts, (c) prototypes.

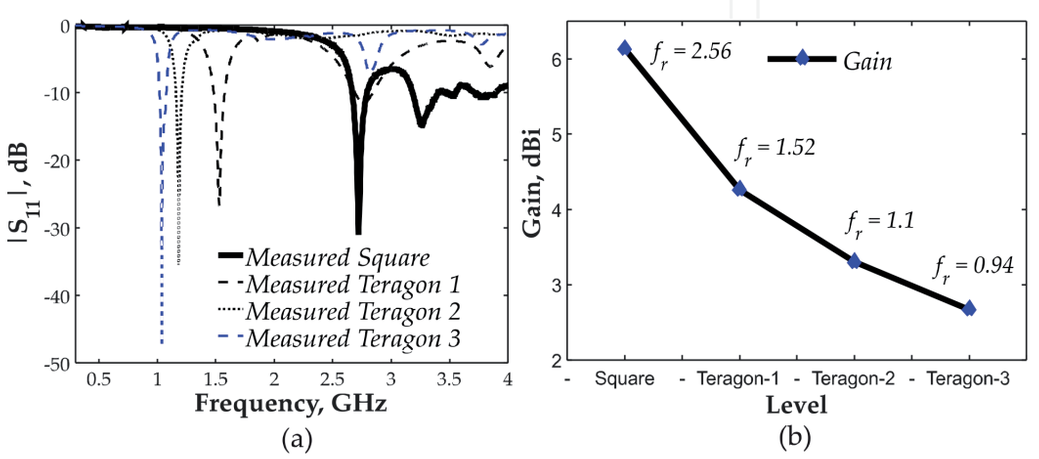

Figure 12.
Results of teragon antenna: (a) measured, (b) gain in dBi.

(a) (b)

Figure 13.
Wearable textile antennas: (a) L-systems, (b) polar transformer.

Several shapes were used in development of the microstrip antennas; the polar transformer is the possibility in this case. **Figure 13** shows the wearable textile antennas: patch generated by L-systems (**Figure 13(a)**) and printed monopole generated by polar transformer, **Figure 13(b)**. Printed monopole antennas (PMA) with polar shape can be observed in several works, operating mainly in the ultra-wideband (UWB), but with projects for 2G, 3G, and 4G technology and X band [35–39]. The altering frequency provided by polar shapes was observed in [38, 40], similar to the observed pre-fractal geometry applied to the PMA [41].

4.3 Polar microstrip antenna

Figure 14 shows frequency resonance of polar microstrip antenna for k-interactions (k = 1, 8 12, 16, 24, 32, 40, 48, 56, 64) and the comparison of measured

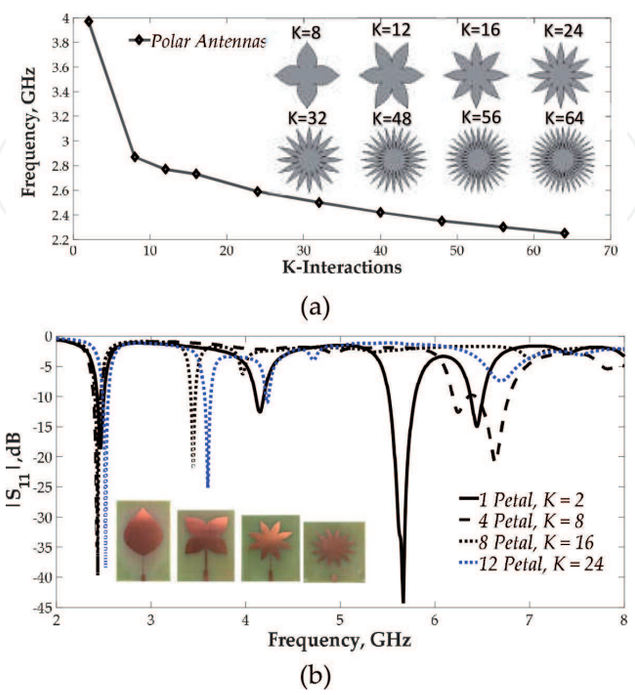

Figure 14.
Interactions of polar microstrip patch antenna: a) comparison of frequency resonance simulated; b) comparison of measured antennas.

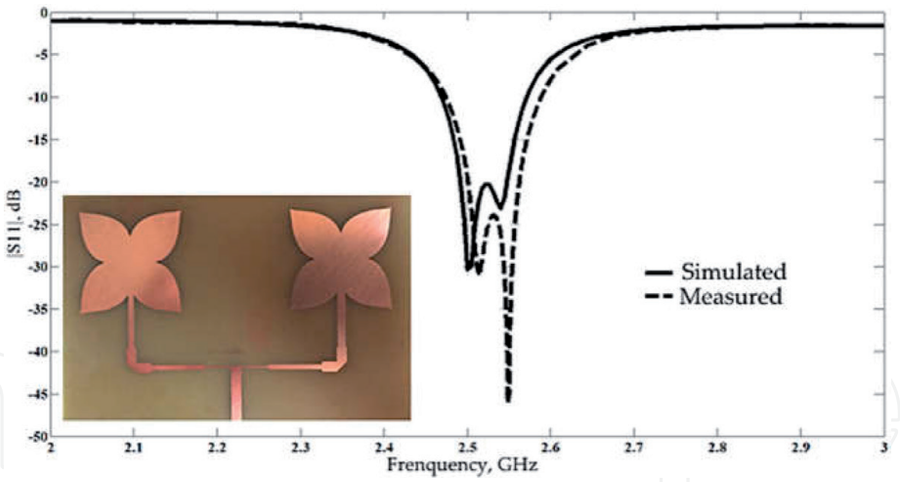

Figure 15.
Polar microstrip patch antenna array with two elements.

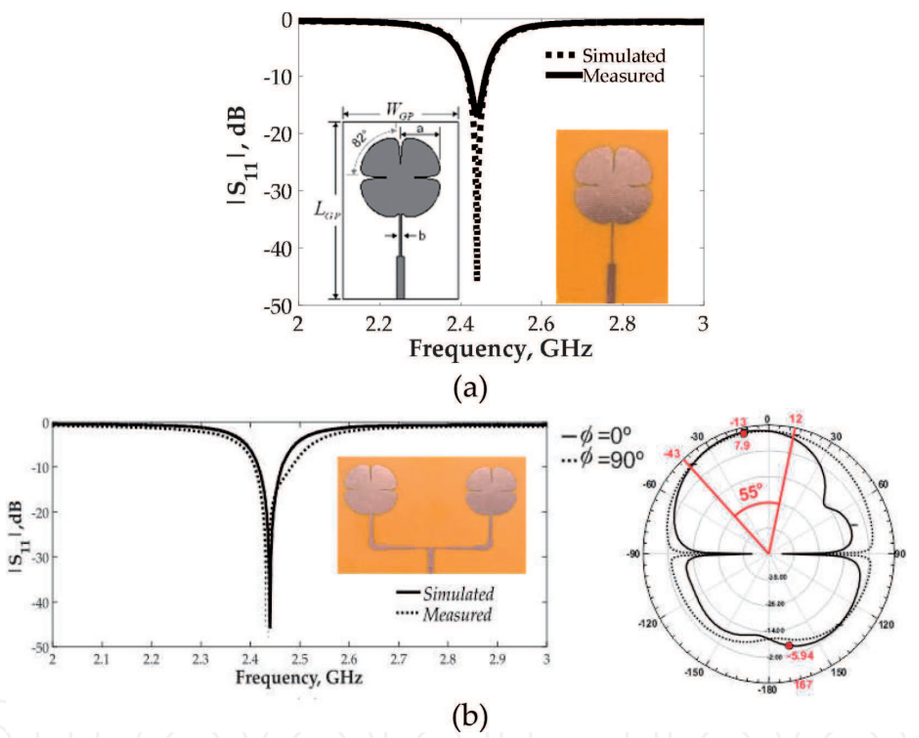

Figure 16.
Polar leaf clover patch antennas: (a) four petals, (b) array of two elements with four petals.

|S11| parameter, with prototype images. The proposed polar patch antennas are based on a circle patch antenna with displaced microstrip line feed, and quarter-wave transformer, with dimensions calculated according [7, 9].

Figure 14 shows the |S11| parameters measured by the polar antennas to k = 2, 8, 16, 24. We noted than the increase of the patch perimeter by the use of polar interaction provides a reduction of the resonant frequencies, similar to the fractal comportment. The greater difference can be observed in k = 2 and k = 8, of 3.4 GHz, and all structures with dual-frequency resonances.

Figure 15 shows the use of polar transformer in the development of the array patch antenna with 4 petals, k = 8 interactions. The polar array presented good response, with simulated and measured results closed, had loss return less than −45 dB and bandwidth of 101 MHz, and covered the WLAN band in 2.4 GHz.

The other shape used was the leaf clover, generated by (8). **Figure 16** shows the comparison of $|S_{11}|$ parameter measured and simulated with leaf clover with four and

six petals for one and two patch elements and prototype images; **Table 3** presents the dimensions used. The polar antenna with six petals presented great bandwidth (52 MHz) than the polar antenna with four petals (42 MHz) and best loss return (−26.3 dB), **Figure 13(b)**.

$$r = 4.4 - \min\left(abs\left(\tan\left(2t + \pi/1\right)\right)/10, 3\right) \tag{6}$$

From the leaf clover antennas, polar array patch antennas with two and four elements have been developed. **Figure 16** shows polar array patch antennas with the shape of clover of four and six petals, with two and four elements, operating in WLAN range. The antennas presented measured bandwidth of 81 MHz and half power beamwidth (HPBW) of 55°, the inclination of radiation pattern indicating the great element used in the patch array (**Figure 17**).

Figure 18 shows the Koch fractal patch antenna array with two elements of the square geometry until Koch level 2. The applications of Koch fractal in the array

Antenna	***L_{GP}***	***W_{GP}***	***a***	***b***
4 Petals	58,83	38,22	14,12	0,56
6 Petals	58,83	38,22	14,15	0,44

Table 3.
Dimensions of leaf clover antenna (mm).

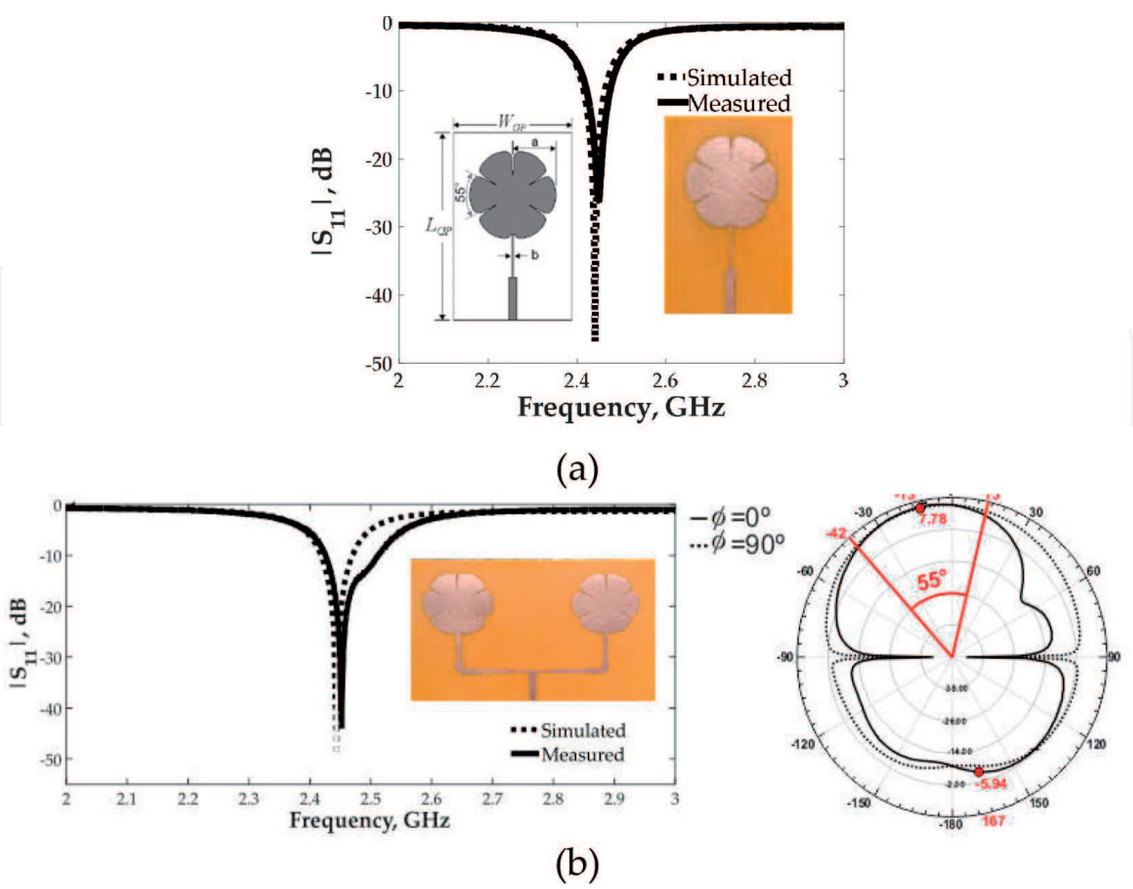

Figure 17.
Polar leaf clover patch antennas: (a) six petals, (b) array of two elements with six petals.

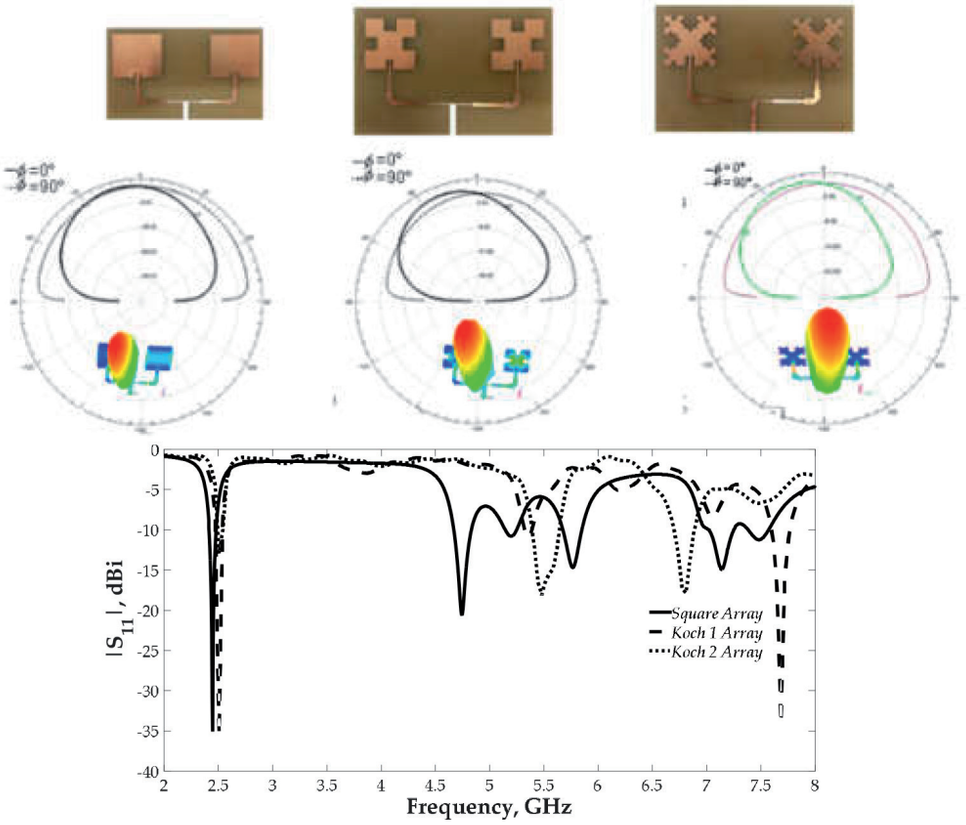

Figure 18.
Koch array patch antenna with two elements.

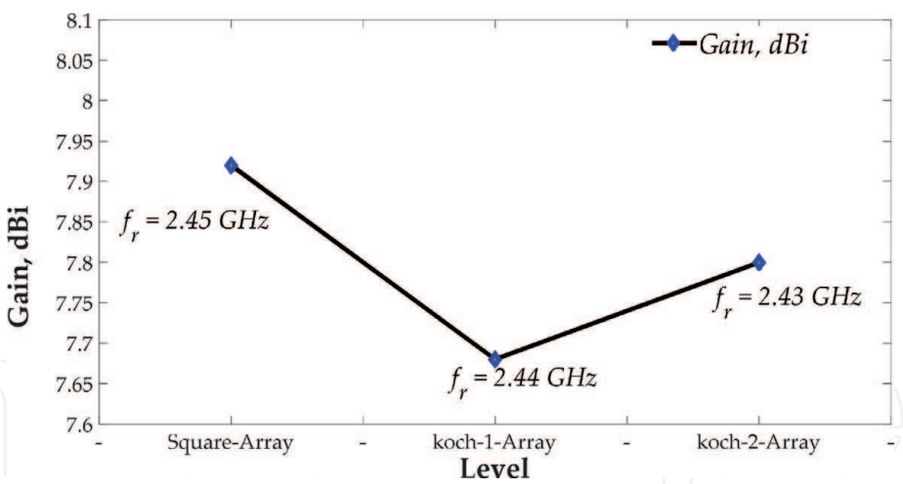

Figure 19.
Gain comparison of the Koch array patch antenna with two elements.

structure provide great bandwidth (113 MHz) and maximum gain in end-fire direction of 7.93 dBi (**Figure 19**), with variation of radiation pattern, indicating lager patch element.

5. Conclusions

In this chapter, we have described some trends for the computer-aided design of microstrip antennas (patches and printed monopoles) for wireless sensors network applications. With the use of such CAD tools, innovative designs of antennas and arrays with pre-fractals and polar motifs were approached and

their properties checked. The methods of analysis, manufacturing, and measurement have been presented considering different dielectric materials (rigid and flexible) for the manufacture of the antennas. The proposed antennas have been fed by microstrip line, and different feeding techniques have been considered for matching impedances and suppression of harmonic frequencies. The unique properties of space-filling and self-similarity naturally result in more compact and multiband behavior antennas. On the other hand, it is verified from the presented results that the polar elements (like a Rosacea of n-petals) also present the property of space-filling, resulting in more compact antennas. On the other hand, pre-fractals and polar patch antennas generally have their gain and/or bandwidth reduced as the number of iterations increases, which in many wireless applications are undesirable characteristics. To overcome these limitations, we proposed the design of fractals and polar arrangements with dissimilar elements, which allows increasing the bandwidth and gain of simple antennas. Further developments included the design of printed monopole antennas for ultra-wideband applications. Flexible substrates (polyamide and denim) were used in the design of wearable antennas with esthetic appeal. The microstrip antennas with pre-fractals and polar elements have few design variables and smooth responses in the region of interest, which facilitates all steps of the design methodology.

Acknowledgements

This work was supported by CNPq under contracts 472098/2013-6 and 308509/2015-3, by the Federal Institute of Paraíba (IFPB), Federal University of Campina Grande (UFCG), State University of Paraíba (UEPB), State University of Maranhão, and FAPEMA.

Author details

Paulo Fernandes da Silva Junior[1*], Mauro Sérgio Pinto Silva Filho[1], Ewaldo Eder de Carvalho Santana[1], Paulo Henrique da Fonseca Silva[2], Elder Eldervitch Carneiro de Oliveira[3], Maciel Alves de Oliveira[4], Fabrício Ferreira Batista[4], Alexandre Jean René Serres[4], Raimundo Carlos Silvério Freire[4], Almir Souza, Silva Neto[5], Severino Aires de Araújo Neto[6]and Carlos Augusto de Moraes Cruz[7]

1 State University of Maranhão, São Luís, Brazil

2 Federal Institute of Paraíba, João Pessoa, Brazil

3 Estadual University of Paraíba, João Pessoa, Brazil

4 Federal University of Campina Grande, Campina Grande, Brazil

5 Federal Institute of Education, Science and Technology of Maranhão, São Luís, Brazil

6 Federal University of Paraíba, João Pessoa, Brazil

7 Federal University of Amazonas, Manaus, Brazil

*Address all correspondence to: paulo.junior@ee.ufcg.edu.br

References

[1] Elfergani I, Hussaini AS, Rodriguez J, Abd-Alhameed R. Antenna Fundamentals for Legacy Mobile Applications and beyond. USA: Springer; 2018. DOI: 10.1007/978-3-319-63967-3

[2] LeMoyne R, Mastroinanni T. Wearable and Wireless Systems for Healthcare I. Singapore: Springer; 2018. DOI: 10.1007/978-981-10-5684-0

[3] Chen ZN, Chia MYW. Broadband Planar Antennas: Design and Applications. Chichaster, England: John Wiley & Sons, Ltd; 2006

[4] Peres A. Wi-Fi Integration to the 4G Mobile Network. Hoboken, USA: John Wiley & Sons; 2018

[5] Yang Y, Shi JXG, Wang CX. 5G Wireless Systems: Simulations and Evaluation Techniques. Switzerland: Springer; 2018. DOI: 10.1007/978-3-319-61869-2

[6] http://www.4gamericas.org/files/6514/3930/9262/4G_Americas_5G_Spectrum_Recommendations_White_Paper.pdf

[7] Balanis CA. Antenna Theory. 3rd ed. Arizona: Wiley; 2009. p. 941

[8] Garg R, Bhartia P, Bahl I, Ittipiboon A. Microstrip Antenna Design Handbook. Boston, USA: Artech House; 2001

[9] Stutzman WL. Antenna Theory and Design. 2nd ed. New York: John Wiley & Sons; 1998. p. 598

[10] Kumar G, Ray KP. Broadband Microstrip Antennas. Boston, Mass, USA: Artech House; 2003

[11] Milligan TA. Modern Antenna Design. 2nd ed. New Jersey, USA: John Wiley & Sons, Inc.; 2005

[12] Federal Communications Commission. Revision of Part 15 of the Commission's Rules Regarding Ultra-Wideband Transmission Systems, First Report and Order (ET Docket 98-153), Adopted Feb. 14, 2002, Released Apr. 22, 2002

[13] Oliveira EEC, Silva PHF, Campos ALPS, d'Assunção AG. Small-size quasi-fractal patch antenna using the Minkowski curve. Microwave and Optical Technology Letters. 2010;**52**(4):805-809. DOI: 10.1002/mop

[14] Deschamps G, Sichak W. Microstrip microwave antennas. In: Proceedings of the Third Symposium on the USAF Antenna Research and Development Program; 1953. pp. 18-22

[15] Byron EV. A new flush-mounted antenna element for phased array application. In: Proc. Phased-Array Antenna Symp.; 1970. pp. 87-192

[16] Munson RE. Conformal microstrip antennas and microstrip phased arrays. IEEE Transactions on Antennas and Propagation. 1974;**22**(1):74-78. DOI: 10.1109/TAP.1974.1140723

[17] Chong C, Watanabe F, Inamura H. Potential of UWB technology for the next generation wireless communications. In: IEEE Ninth International Symposium on Spread Spectrum Techniques and Applications; 2006. pp. 422-429. 10.1109/ISSSTA.2006.311807

[18] Cohen N. Fractal antenna applications in wireless telecommunications. Proceedings of Electronics Industries Forum of New England. 1997:43-49

[19] Oliveira EEC, Silva PHF, Campos ALPS, Silva SG. Overall size antenna reduction using fractal elements. Microwave and Optical Technology

Letters. 2009;**51**(3):671-675. DOI: 10.1002/mop

[20] Howell JQ. Microstrip antennas. IEEE Transactions on Antennas and Propagation. 1974;**23**(1):90-93. DOI: 10.1109/TAP.1975.1141009

[21] Werner DH, Ganguly S. An overview of fractal antenna engineering research. IEEE Antennas and Propagation Magazine. 2003;**45**(1):38-57. DOI: 10.1109/MAP.2003.1189650

[22] The Antenna Company International. [Internet]. 2010. Available from: http://www.antennacompany.com [Accessed: 11 August 2015]

[23] Silva MR, Nóbrega CL, SILVA PHF, D'Assuncao AG. Optimal design of frequency selective surfaces with fractal motifs. IET Microwaves, Antennas and Propagation. 2014;**1**(9):1-5. DOI: 10.1049/iet-map.2013.0462

[24] Silva MR, Nóbrega CL, SILVA PHF, D'Assuncao AG. Optimization of FSS with Sierpinski island fractal elements using population-based search algorithms and MLP neural network. Microwave and Optical Technology Letters. 2014;**56**(4):827-831. DOI: 10.1002/mop.28214

[25] Kassem H, Vigneras V, Lunet G. Characterization techniques for materials' properties measurement. In: Minin I, editor. Microwave and Millimeter Wave Technologies from PhotonicBandgap Devices to Antenna and Applications. Rijeka: InTech; 2010. pp. 289-314

[26] Sheen DM, Ali SM, Abouzahra MD, Kong JA. Application of the three-dimensional finite-difference time-domain method to the analysis of planar microstrip circuits. IEEE Transactions on Microwave Theory and Techniques. 1990;**38**(7):849-857. DOI: 10.1109/22.55775

[27] Sullivan DM. Electromagnetic Simulation Using the FDTD Method. 2nd ed. Piscataway: IEEE Press; 2013. 182 p

[28] Mandelbrot BB. The Fractal Geometry of Nature. 3rd ed. Nova York: W. H. Freeman and Co.; 1982. p. 468

[29] Falconer K. Fractal Geometry: Mathematical Foundations and Application. 2nd ed. Londres: Wiley; 2003. p. 337

[30] Mishra J, Mishra S. L-Systems Fractals. Amsterdam, Netherlands: Elsevier; 2007. p. 274

[31] Barnsley M. Fractals Everywhere. San Diego: Academic Press; 1988. p. 394

[32] Lindenmayer A. Mathematical models for cellular interaction in development, parts I and II. Journal of Theoretical Biology. 1968;**18**(3):280-315. DOI: 10.1016/0022-5193(68)90080-5

[33] Oliveira EEC, Campos ALPS, Silva PHF. Quasi-Fractal Koch Triangular Antenna. In: 2009 SBMO/IEEE MTT-S International Microwave and Optoelectronics Conference (IMOC); 3-6 November; Belém. IEEE; 2009. pp. 163-166. DOI: 10.1109/IMOC.2009.5427607

[34] Silva PHF, Oliveira EEC, d'Assunção AG. Using a multilayer perceptrons for accurate modeling of quasi-fractal patch antennas. In: 2010 International Workshop on Antenna Technology (iWAT) Lisbon; 2010. pp. 1-4. DOI: 10.1109/IWAT.2010.5464782

[35] da Silva PF, Freire RCS, Serres AJR, Silva PHDF, e Silva JC. Bio-inspired antenna for UWB systems. In: 2016 1st International Symposium on Instrumentation Systems, Circuits and Transducers (INSCIT); Belo Horizonte; 2016; pp. 153-157. DOI: 10.1109/INSCIT.2016.7598210

[36] de Moura LCM, Cruz JDN, da Costa AP, Silva PHDF, e Silva JC. UWB cotton leaf design microstrip-fed printed monopole antenna. In: 2015 SBMO/IEEE MTT-S International Microwave and Optoelectronics Conference (IMOC) Porto de Galinhas; 2015. pp. 1-4. DOI: 10.1109/IMOC.2015.7369155

[37] Lemos NA, Silva AN, Paiva HF, Silva PHF. Four-Leaf Clover UWB Planar Monopole Antenna, MOMAG 2014: 16 SBMO. Brazil, 1 CD. 2014

[38] Silva Junior PF, Freire RCS, Serres AJR, Silva PHF, Silva JC. Wearable textile bioinspired antenna for 2G, 3G and 4G systems. Microwave and Optical Technology Letters. 2016;**58**(12): 2818-2823. DOI: 10.1002/mop

[39] Silva PF Jr, Silva PHDF, Serres AJR, Silva JC, Freire RCS. Bio-inspired design of directional leaf-shaped printed monopole antennas for 4G 700 MHz band. Microwave and Optical Technology Letters. 2016;**58**(12): 1529-1533. DOI: 10.1002/mop.29853

[40] Silva Júnior PF, Serres AJR, Freire RCS, Serres GKF, Gurjão EC, Carvalho JN, et al. Bio-inspired wearable antennas. In: Ortiz JH, editor. Wearable Technologies. Rijeka: IntechOpen; 2018. DOI: 10.5772/intechopen.75912

[41] Silva MR, Nóbrega CL, Silva PHF, D'Assunção AG. A new configuration of planar monopole quasi-fractal antenna for wireless communications. In: Digests of the 2010 14th Biennial IEEE Conference on Electromagnetic Field Computation; 9-12 May; Chicago. IEEE; 2010. pp. 1-1. DOI: 10.1109/CEFC.2010.5481786